LANGMUIR Article
Cite This: Langmuir 2019, 35, 4146–4151
pubs.acs.org/Langmuir

Interaction of Anionic Bulk Nanobubbles with Cationic Liposomes: Evidence for Reentrant Condensation

Minmin Zhang and Serge G. Lemay*

MESA+ Institute for Nanotechnology & Faculty of Science and Technology, University of Twente, P.O. Box 217, 7500 AE Enschede, The Netherlands

ABSTRACT: We investigated the interaction of bulk nanobubbles with cationic liposomes composed of 1,2-dioleoyl-*sn*-glycero-3-ethylphosphocholine and anionic liposomes assembled from 1-palmitoyl-2-oleoyl-*sn*-glycero-3-phospho-(1′-*rac*-glycerol). We employed dynamic light scattering and fluorescence microscopy to investigate both the hydrodynamic and electrophoretic properties of the nanobubble/liposome complexes. These optical techniques permit direct visualization of structural changes as a function of the bubble/liposome ratio. We observed reentrant condensation with cationic liposomes and gas nucleation with anionic liposomes. This is the first report of charge inversion and reentrant condensation of cationic liposomes induced by bulk nanobubbles.

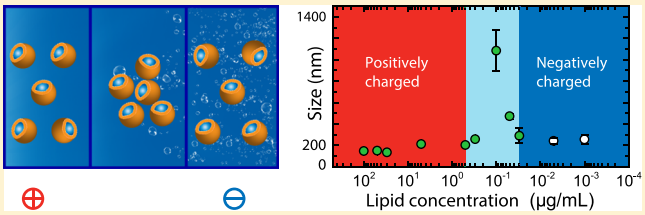

INTRODUCTION

Interaction of gas bubbles with nanoparticles has been studied both experimentally and theoretically by several authors[1−3] owing to its relevance in different areas. These range from biomedical applications, such as ultrasound contrast agents in biomedical imaging and drug delivery, to industrial processes that include mineral separation using froth flotation techniques and waste water treatment.[4−12] However, to our knowledge, no systematic attempt has been devoted to investigating the phenomenology of interactions of bulk nanobubbles with both inorganic and organic nanoparticles and to clarifying the basic mechanism that causes the interaction. Recent investigations, by our group, of the interaction of gas bubbles with colloidal nanoparticles have led to surprising findings including the formation of bubble−nanoparticle complexes[13] and reentrant condensation of positive colloidal nanoparticles.[14]

Liposomes, artificial vesicles whose typical sizes range from 20 nm to micrometers in diameter, are closed shells of self-assembled phospholipid bilayers that surround an aqueous core and are employed as model systems for studying the physical properties of biological membranes.[15] Cationic liposomes have also recently received much interest as a delivery system for DNA and protein vaccines.[16−22] They have become a popular gene transfer agent and have been used as an alternative nonviral DNA delivery vector for gene therapy because of their low toxicity, biodegradability, nonimmunogenicity, and easy preparation.[16,19] However, these nonviral complexes are reported to be rapidly cleared from circulation as a result of enzymatic digestion of plasmid DNA and, in some cases, the phospholipids undergoing oxidation and a hydrolysislike reaction.[18,23,24] It is a major requirement for cationic liposome-mediated transfection to maintain the colloidal stability of the liposome/DNA complex (lipoplex), which is particularly difficult to achieve at the high DNA concentrations used for in vivo studies and clinical trials.[16,20] To stabilize the liposome/DNA particles formed at high DNA concentration and thus prolong the circulation time of lipoplexes in blood, polymers such as protamine and poly(ethylene glycol) (PEG) have been used.[20,24] Despite these achievements, however, both protamine and PEG are reported to have toxicity effects.[25−27] Adverse allergic responses to protamines, including hypotension, bronchospasm, rash, urticaria, cardiovascular collapse, and sometimes death, have been reported.[28,29] PEG and PEG-related polymers are often sonicated when used in biomedical applications. Murali et al. reported that when sonicated, PEG is very sensitive to sonolytic degradation and PEG degradation products are toxic to mammalian cells.[27]

Here, we investigated the modulation effect of gas nanobubbles on the stability of both cationic and anionic liposomes. The schematic illustration of a single liposome is shown in Figure 1a. Figure 1b,c show the molecular structures of the phospholipids employed to create the cationic liposomes and anionic liposomes, respectively. We present a comprehensive study of the interaction between cationic liposomes and gas nanobubbles by combining dynamic light scattering (DLS) and fluorescence microscopy measurements. We find that the charge and colloidal stability of cationic phospholipid liposomes can be influenced by gas bubble solutions with the cationic liposomes undergoing a reentrant condensation process upon interaction with nanobubbles. Our motivation is that, compared with flexible polymers, gas nanobubbles do not require chemical modification and spontaneously dissipate over time, yet still allow tuning the surface charge of liposomes and shield them from the extracellular environment.

Received: November 23, 2018
Revised: February 25, 2019
Published: February 27, 2019

DOI: 10.1021/acs.langmuir.8b03927
Langmuir 2019, 35, 4146–4151

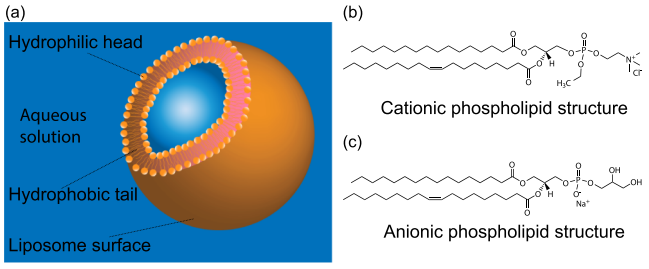

Figure 1. (a) Schematic illustration of self-assembled lipid bilayer liposomes in aqueous solution. (b) Molecular structure of cationic phospholipid, 1,2-dioleoyl-*sn*-glycero-3-ethylphosphocholine (EDOPC) employed to form cationic liposomes. (c) Molecular structure of anionic phospholipid, 1-palmitoyl-2-oleoyl-*sn*-glycero-3-phospho-(1′-*rac*-glycerol) (POPG) used to create anionic liposomes.

RESULTS AND DISCUSSION

Reentrant Condensation of Cationic Liposomes with Nanobubbles. Colloidal stability of liposomes is a primary requirement for cationic liposome-mediated gene transfection.[30] Therefore, we used DLS to assess both the hydrodynamic size distribution and electrophoretic properties of bubble/liposome complexes mixed at a series of lipid concentrations ranging from 0.1 mg/mL to 1 ng/mL, as presented in Figure 2. The average size of the nanobubble/EDOPC complexes remained essentially constant (i.e., on the order of 200 nm) until a critical coalescence concentration (C^*) of ~0.5 μg/mL was reached. Below this concentration, a gradual increase in size was observed up to a concentration of 0.1 μg/mL, at which point, coalescence of complexes occurred, leading to structures larger than 1 μm in diameter. As the lipid concentration was further decreased, a remarkable transition back toward smaller size was observed, where the increase in the relative concentration of the gas solution started to restabilize the large aggregates. Once the lipid concentration reached a second critical coalescence concentration (C^{**}) of ~0.03 μg/mL, the complex size became once again essentially constant at a value close to that at high lipid concentration. This indicates that upon further decreasing the lipid concentration, the colloidal stability of the EDOPC complexes was restored. Note that once the lipid concentration was decreased down to 0.01 μg/mL, the measurements were near the detection threshold of the DLS instrument, which may introduce some systematic error (to emphasize this, the last two data points are plotted as open symbols in Figure 2).

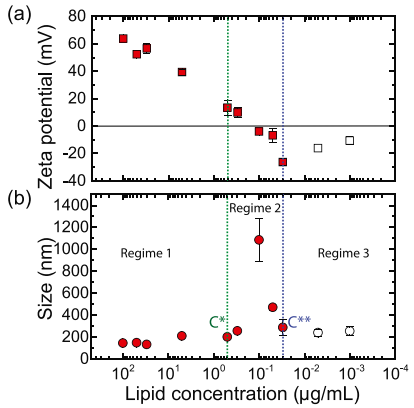

Figure 2. (a) Average zeta potential and (b) hydrodynamic diameter of the bubble/liposome (100 nm) complexes as a function of EDOPC concentration. Size determination was performed after 1 min of ultrasonication at room temperature. C^* and C^{**} are two critical coalescence concentrations (CCC) separating the graph into three different regimes and were determined empirically. Error bars which are smaller than the symbol size are not shown.

On the basis of earlier measurements with positively charged nanoparticles, it may be expected that the presence of nanobubbles influences the charge state of cationic liposomes. To test this hypothesis, we performed zeta potential measurements, a quantity that is directly related to the surface charge of the particles. Figure 2 shows the average zeta potential of the nanobubble/EDOPC complexes as a function of lipid concentration. A clear inversion of the surface charge from positive to negative is observed upon decreasing the cationic liposome concentration. That is, the point of (effective) zero charge (~0.1 μg/mL) lies in between the critical coalescence concentrations, C^* and C^{**}. The presence of large particles is presumably due to liposome coalescence. This indicates that the effect of the nanobubble solution is to neutralize the surface charge of the cationic liposomes, presumably because of nucleation at the liposome surface,[13] leading to a loss of colloidal stability and coalescence of the liposomes into large aggregates.

We thus find that the nanobubble/liposome complexes exhibit a three-regime model of colloidal stability, as shown in Figure 2, in which regimes 1 and 3 are characterized as highly positive and negative colloidal stable bubble/EDOPC systems, respectively, whereas regime 2 corresponds to colloidally unstable bubble/liposome aggregates. This phenomenon is known as reentrant condensation.[31,32]

To further confirm that coalescence is indeed due to nanobubble/liposome interactions, we performed DLS and zeta potential measurements on control samples, where the liposome solution was mixed with an untreated 10 mM NaCl solution. All other parameters were kept the same as the measurements with hydrolysis-treated electrolyte presented above. The results are shown in Figure 3. In contrast to the nanobubble/EDOPC mixtures, the particle size remained essentially constant (on the order of 200 nm) and no agglomeration occurred for salt/EDOPC. The zeta potential remained positive over the concentration range where the nanobubble solution exhibited reentrant condensation. The

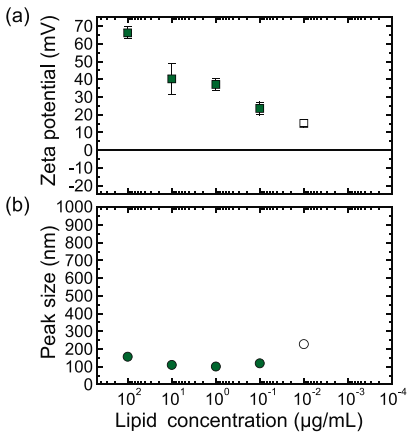

Figure 3. Control experiments: (a) average zeta potential and (b) hydrodynamic diameter of the salt/liposome mixtures as a function of lipid concentration.

DOI: 10.1021/acs.langmuir.8b03927
Langmuir 2019, 35, 4146−4151

decline of zeta potential with decreasing lipid concentration has been attributed to experimental artifact.[33−35] For example, Tantra et al. observed a shift in zeta potential values to less negative values for nanoparticle suspensions at extreme dilution, which they attributed to an increase in the signal arising from extraneous particulate matter.[33]

To further elucidate the interaction between nanobubbles and cationic liposomes, the structure of the nanobubble/liposome complexes at several representative EDOPC concentrations was visualized by fluorescence microscopy. Figure 4a shows the fluorescence image of the 1 mg/mL source

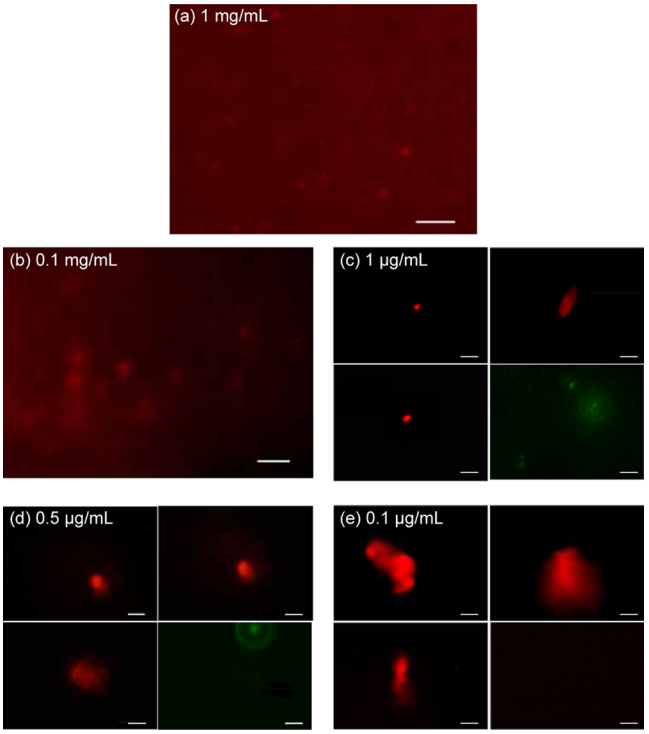

Figure 4. Fluorescence microscopy of nanobubble/EDOPC liposome complexes labeled with Texas Red dye at representative lipid concentrations. (a) Source EDOPC liposome solution with a concentration of 1 mg/mL before interacting with the nanobubbles. The uniform red background is due to contributions from out-of-focus liposomes in this high concentration solution. (b,c) Bubble/EDOPC complexes at lipid concentrations before critical coalescence concentration C^*. (d) Nanobubble/EDOPC complexes at lipid concentration near C^*. (e) Nanobubble/EDOPC complexes at lipid concentration of 0.1 μg/mL, at which significant coalescence occurred. The scale bars represent 5 μm. In (c−e), the density of spots was too low to allow visualizing several in a single frame. Therefore, three representative images of individual complexes are shown. In each case, the bottom right panel (green) is a control experiment in which EDOPC liposomes were mixed with a nanobubble-free solution. The observed spots are resolution limited except in panels (d,e). The intensity scale at each concentration has been rescaled for clarity and intensities thus cannot be directly compared.

solution of cationic liposomes before mixing with the nanobubble solution. A nearly uniform red background is observed, which is due to the large concentration of out-of-focus fluorescently labeled liposomes. A few bright spots are also observed, corresponding to individual liposomes in the focus plane of the microscope. These spots are resolution limited, therefore the size of the liposomes cannot be inferred from these fluorescence images. By gradually decreasing the cationic liposome concentration via mixing with the nanobubble solution, the uniform background fades (Figure 4b) until only discrete entities can be discerned against a dark background (Figure 4c−e). Below the critical coalescence concentration of C^* (Figure 4d), objects larger than the resolution limit begin to appear, increasing further in size at lower concentrations (Figure 4e). This behavior is consistent with the DLS measurements, which exhibit a marked increase in the hydrodynamic diameter in the same concentration range. In contrast, control measurements in which untreated NaCl solution is used instead of nanobubble solution to dilute the liposome solution show no such aggregation behavior (green images in Figure 4c−e). The control measurement in Figure 4e (bottom right panel) shows only a black background. This is because at a low lipid concentration of 0.1 μg/mL, it is practically impossible to capture the objects. The aggregates, on the other hand, are large and diffuse more slowly, and therefore can be manually tracked even at low concentrations. For the same reason, systematic fluorescence measurements at concentrations below C^{**} proved to be impractical due to the rarity of the events.

Taken together, the phenomenology of reentrant condensation of cationic liposomes can be summarized in a charge inversion scenario similar to our previous work on positive amidine nanoparticles. That is, we propose that the supersaturated solution causes the formation of gas bubbles on the surface of the liposomes, screening out the positive liposome surface charge and exhibiting a negative surface charge to the solution. Near the point of zero charge, this renders the colloidal suspension unstable. Further decreasing the lipid concentration causes the net surface charge to reverse sign, which becomes colloidally stable again.

Interactions of Nanobubbles with Anionic Liposomes. We also looked at the interaction between nanobubbles and anionic liposomes in the same concentration range as for cationic liposomes. As shown in Figure 5, the zeta potential of the nanobubble/DOPG complexes remained negative with a gradual decline in magnitude (from very negative to less negative, Figure 5a), whereas the size slightly increased (Figure 5b), consistent with a gas layer nucleating onto a liposome surface. This behavior is highly reminiscent of

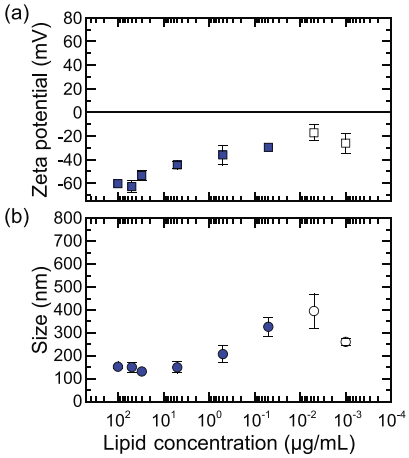

Figure 5. Interaction of nanobubbles with anionic liposomes: (a) average zeta potential and (b) hydrodynamic diameter of nanobubble/POPG complexes as a function of POPG concentration.

DOI: 10.1021/acs.langmuir.8b03927
Langmuir 2019, 35, 4146−4151

our earlier measurements on gold nanoparticles,[13] which were interpreted as resulting from bubble nucleation on the nanoparticle surface.

In this interpretation, the decrease in magnitude of the zeta potential occurs because the bubbles are less negative than the anionic liposomes. They can thus shield the strong negative charge of the anionic liposomes, resulting in a decrease of net surface charge for the bubble/DOPG complexes. These results are thus again consistent with our hypothesis that nanobubble nucleation at the liposome surface accounts for the bubble−liposome interaction.

CONCLUSIONS

We have presented the first experimental observations of reentrant condensation of model cationic liposomes in bulk solution under the influence of anionic nanobubbles using both microscopy and size measurements. Zeta potential measurements indicate that this coincided with surface charge inversion. On the basis of the observations, we propose a mechanism of gas nucleation on the liposome surfaces to address the bubble/liposome interactions. Bubbles nucleate on the liposome surfaces and thus screen their surface charge, leading to a shift or even reversal of the sign of the zeta potential. These observations provide a new pathway to tune liposome interactions in solution. Further studies are needed to establish whether these results can be generalized to vesicle separation techniques and delivery systems. From the medical application point of view, for example in blood, usefulness depends on how long it takes the nanobubbles to dissipate. As kinetic data for nanobubbles are currently lacking, further studies are needed to address this aspect. This is of particular interest for the growing number of studies that isolate and manipulate liposomes, providing a new mechanism that does not require chemical modification and by which they can be redissolved over time.[36,37]

MATERIALS AND METHODS

Materials. POPG (sodium salt, >99%) and EDOPC (chloride salt, >99%) were purchased from Avanti (Avanti Polar Lipids, Inc. USA) and were used without further purification. NaCl at a 10 mM concentration was prepared using water from Milli-Q system (Millipore, USA) with resistivity of 18.2 MΩ cm at 25 °C. The pH of the sodium chloride solution was not explicitly controlled and had a measured value of 6.5. Texas Red-modified 1,2-dihexadecanoyl-*sn*-glycero-3-phosphoethanolamine(triethylammonium salt) (Texas Red DHPE) was supplied by Thermo Fisher Scientific and was prepared at a concentration of 0.2 mg/mL.

Liposome Preparation via Extrusion. All of the liposomes were prepared via a mechanical extrusion method. EDOPC and POPG were first dissolved in chloroform forming a clear homogeneous lipid solution at 10 mg/mL. The fluorescence-labeled liposome was produced by mixing the target phospholipid with Texas Red DHPE at a mass ratio of 1000 phospholipid to 1 red fluorescent dye, allowing maximum contrast in fluorescent microscope imaging. The stock solution (10 mg/mL, 99.9 μL) and Texas Red DHPE (0.2 mg/mL, 4.4 μL) were transferred into a clean glass vial using glass syringes with a metal needle. The organic solvent was evaporated using a dry nitrogen stream in a fume hood to yield a uniform lipid film. The lipid film was thoroughly dried to remove the residual chloroform by placing the glass vial under vacuum for 1 h. The dry lipid film was then resuspended in 1 mL NaCl aqueous solution (10 mM) to a final lipid concentration of 1 mg/mL, and vortexed for ∼1 min above the phase transition temperatures, T_c, of the lipids (−2 °C for POPG and −17 °C for EDOPC). The resulting lipid suspension was extruded 11 times through 0.1 μm polycarbonate membranes using a Mini Extruder (Avanti Polar Lipids, Inc. USA). Finally, a homogeneous liposomal suspension of uniformly sized unilamellar vesicles with an average diameter of 116 ± 8 nm (nominally 100 nm) was obtained. The final solution was wrapped in aluminum foil and kept in the dark in a refrigerator at 4 °C.

Nanobubble Generation and Characterization. The nanobubble solutions were generated via high-power water electrolysis in a cell consisting of planar Pt electrodes with an area of ∼66 cm^2. NaCl aqueous solution (10 mM) was pressure-driven through the cell at a flow rate of 500 mL/min and treated with a cell voltage of 24 V and an average current of 3.0 A. As a result, water was decomposed into oxygen and hydrogen gas, which became dissolved in the water stream. Through this process, the solution becomes supersaturated with oxygen and hydrogen gas. Stable nanosized colloidal objects, commonly referred to in the literature as nanobubbles,[38−41] were observed in the supersaturated solutions following water electrolysis.

Characterization of the nanobbubble solution was carried out by DLS for sizing and electrophoresis for zeta potential determination, both conducted at 25 °C with the help of a Malvern Zetasizer Nano ZS equipped with a laser (633 nm) set at an angle of 173°. Detailed operating parameters of each technique were selected for consistency with earlier work.[13] In short, the average and standard deviation of five measurements were computed for further analysis. Measurements of our nanobubble solutions exhibited a peak size and full width at half maximum of 223 and 94−529 nm, respectively, and a negative charge with a mean zeta potential of −19 ± 3 mV. The nanobubbles are negatively charged over a broad range of pH as shown in Figure 6.

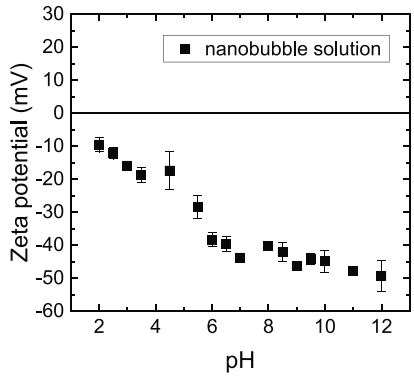

Figure 6. Zeta potential of the nanobubble solutions as a function of pH in 10 mM NaCl at 25 °C.

Nanoparticle tracking analysis (NTA, NS500, Nanosight, Malvern Instruments) was used to measure the concentration. NTA is able to directly count the number of tracked particles in a known volume, which gave a concentration of ∼10^7 to 10^8 /mL for our nanobubble solution. The solution exhibited long term stability as reported in our previous work on the interaction of nanobubbles with solid-state nanoparticles.[13]

Particle Size and Zeta Potential Determination. All measurements were conducted in 10 mM NaCl (pH 6.5) as the reference system. DLS and electrophoresis measurements were once again applied for the determination of hydrodynamic diameter and zeta potential of the liposome/bubble mixtures, respectively. The signal analysis was performed using the software provided by the manufacturer (Zetasizer Software, Malvern). The interaction of anionic nanobubbles with liposomes was initiated by adding the nanobubble solution to an existing liposome suspension to a final volume of 1 mL, followed by gentle mixing and ∼1 min ultrasonication (Branson B200, 120 V). Control experiments studying the difference between nanobubbles before and after ultrasonication yield the same results, which demonstrates negligible influence of mild ultrasonication on nanobubbles. Note that, in the presence of free lipids, the surface properties of bubbles might change to some extent as lipid molecules might associate with bubble surfaces.

DOI: 10.1021/acs.langmuir.8b03927
Langmuir 2019, 35, 4146−4151

Fluorescence Microscopy Imaging. A fluorescent microscope (Olympus, IX71) equipped with a powerful 120 W lamp (X-Cite 120PC Q) as an excitation light source and a digital camera (Olympus, DP70) for image acquisition was used to visualize and image the structure of the nanobubble/liposome complexes at several representative EDOPC concentrations. The Texas Red-labeled samples were exposed to a laser with an excitation wavelength of 595 nm using a filter cube (Olympus, IX2-RFAC). Depending on the lipid concentration, the laser intensity was adjusted to achieve maximum contrast in fluorescent microscopy imaging.

AUTHOR INFORMATION

Corresponding Author

*E-mail: s.g.lemay@utwente.nl.

ORCID

Minmin Zhang: 0000-0002-2211-2850

Notes

The authors declare no competing financial interest.

ACKNOWLEDGMENTS

The author would like to acknowledge Yao Lu for her kind help with liposome preparation, fluorescent microscopy imaging, and useful discussion. The authors thank the Tennant Company for financial support.

REFERENCES

(1) Nguyen, A. V.; Nalaskowski, J.; Miller, J. D. A study of bubble-particle interaction using atomic force microscopy. *Miner. Eng.* **2003**, *16*, 1173−1181.

(2) Meyer, E. E.; Rosenberg, K. J.; Israelachvili, J. Recent progress in understanding hydrophobic interactions. *Proc. Natl. Acad. Sci. U.S.A.* **2006**, *103*, 15739−15746.

(3) Xiao, W.; Ke, S.; Quan, N.; Zhou, L.; Wang, J.; Zhang, L.; Dong, Y.; Qin, W.; Qiu, G.; Hu, J. The Role of Nanobubbles in the Precipitation and Recovery of Organic Phosphine-containing in Beneficiation Wastewater. *Langmuir* **2018**, *34*, 6217−6224.

(4) Xing, Z.; Wang, J.; Ke, H.; Zhao, B.; Yue, X.; Dai, Z.; Liu, J. The fabrication of novel nanobubble ultrasound contrast agent for potential tumor imaging. *Nanotechnology* **2010**, *21*, 145607.

(5) Rapoport, N.; Gao, Z.; Kennedy, A. Multifunctional nanoparticles for combining ultrasonic tumor imaging and targeted chemotherapy. *J. Natl. Cancer Inst.* **2007**, *99*, 1095−1106.

(6) Lukianova-Hleb, E. Y.; Wagner, D. S.; Brenner, M. K.; Lapotko, D. O. Cell-specific transmembrane injection of molecular cargo with gold nanoparticle-generated transient plasmonic nanobubbles. *Biomaterials* **2012**, *33*, 5441−5450.

(7) Bhaskar, S.; Tian, F.; Stoeger, T.; Kreyling, W.; de la Fuente, J. M.; Grazú, V.; Borm, P.; Estrada, G.; Ntziachristos, V.; Razansky, D. Multifunctional Nanocarriers for diagnostics, drug delivery and targeted treatment across blood-brain barrier: perspectives on tracking and neuroimaging. *Part. Fibre Toxicol.* **2010**, *7*, 3.

(8) Xing, Y.; Gui, X.; Cao, Y. The hydrophobic force for bubble−particle attachment in flotation−a brief review. *Phys. Chem. Chem. Phys.* **2017**, *19*, 24421−24435.

(9) Calgaroto, S.; Wilberg, K. Q.; Rubio, J. On the nanobubbles interfacial properties and future applications in flotation. *Miner. Eng.* **2014**, *60*, 33−40.

(10) Uchida, T.; Oshita, S.; Ohmori, M.; Tsuno, T.; Soejima, K.; Shinozaki, S.; Take, Y.; Mitsuda, K. Transmission electron microscopic observations of nanobubbles and their capture of impurities in wastewater. *Nanoscale Res. Lett.* **2011**, *6*, 295.

(11) Agarwal, A.; Ng, W. J.; Liu, Y. Principle and applications of microbubble and nanobubble technology for water treatment. *Chemosphere* **2011**, *84*, 1175−1180.

(12) Temesgen, T.; Bui, T. T.; Han, M.; Kim, T.-i.; Park, H. Micro and nanobubble technologies as a new horizon for water-treatment techniques: A review. *Adv. Colloid Interface Sci.* **2017**, *246*, 40−51.

(13) Zhang, M.; Seddon, J. R. T. Nanobubble−Nanoparticle Interactions in Bulk Solutions. *Langmuir* **2016**, *32*, 11280−11286.

(14) Zhang, M.; Seddon, J. R. T.; Lemay, S. G. Nanoparticle-nanobubble interactions: reentrant condensation of amidine latex nanoparticles driven by bulk nanobubbles. *J. Colloid Interface Sci.* **2019**, *538*, 605−610.

(15) Pencer, J.; White, G. F.; Hallett, F. R. Osmotically induced shape changes of large unilamellar vesicles measured by dynamic light scattering. *Biophys. J.* **2001**, *81*, 2716−2728.

(16) Gao, X.; Huang, L. Potentiation of cationic liposome-mediated gene delivery by polycations. *Biochemistry* **1996**, *35*, 1027−1036.

(17) Barenholz, Y. Liposome application: problems and prospects. *Curr. Opin. Colloid Interface Sci.* **2001**, *6*, 66−77.

(18) Akbarzadeh, A.; Rezaei-Sadabady, R.; Davaran, S.; Joo, S. W.; Zarghami, N.; Hanifehpour, Y.; Samiei, M.; Kouhi, M.; Nejati-Koshki, K. Liposome: classification, preparation, and applications. *Nanoscale Res. Lett.* **2013**, *8*, 102.

(19) Martin, B.; Sainlos, M.; Aissaoui, A.; Oudrhiri, N.; Hauchecorne, M.; Vigneron, J.; Lehn, J.; Lehn, P. The design of cationic lipids for gene delivery. *Curr. Pharm. Des.* **2005**, *11*, 375−394.

(20) Pitard, B.; Oudrhiri, N.; Lambert, O.; Vivien, E.; Masson, C.; Wetzer, B.; Hauchecorne, M.; Scherman, D.; Rigaud, J.-L.; Vigneron, J.-P.; Lehn, J.-M.; Lehn, P. Sterically stabilized BGTC-based lipoplexes: Structural features and gene transfection into the mouse airways in vivo. *J. Gene Med.* **2001**, *3*, 478−487.

(21) Miller, A. D. Cationic Liposomes for Gene Therapy. *Angew. Chem., Int. Ed.* **1998**, *37*, 1768−1785.

(22) Lee, R. J.; Huang, L. Lipidic Vector Systems for Gene Transfer. *Crit. Rev. Ther. Drug Carrier Syst.* **1997**, *14*, 34.

(23) Cullis, P. R. Stabilized plasmid-lipid particles for systemic gene therapy. *Gene Ther.* **2000**, *7*, 1867−1874.

(24) Li, S.; Huang, L. In vivo gene transfer via intravenous administration of cationic lipid−protamine−DNA (LPD) complexes. *Gene Ther.* **1997**, *4*, 891.

(25) Sokolowska, E.; Kalaska, B.; Miklosz, J.; Mogielnicki, A. The toxicology of heparin reversal with protamine: past, present and future. *Expert Opin. Drug Metab. Toxicol.* **2016**, *12*, 897−909.

(26) Kreppel, F.; Kochanek, S. Modification of Adenovirus Gene Transfer Vectors With Synthetic Polymers: A Scientific Review and Technical Guide. *Mol. Ther.* **2008**, *16*, 16−29.

(27) Murali, V. S.; Wang, R.; Mikoryak, C. A.; Pantano, P.; Draper, R. Rapid detection of polyethylene glycol sonolysis upon functionalization of carbon nanomaterials. *Exp. Biol. Med.* **2015**, *240*, 1147−1151.

(28) Chu, Y.-Q.; Cai, L.-J.; Jiang, D.-C.; Jia, D.; Yan, S.-Y.; Wang, Y.-Q. Allergic shock and death associated with protamine administration in a diabetic patient. *Clin. Ther.* **2010**, *32*, 1729−1732.

(29) Porsche, R.; Brenner, Z. R. Allergy to protamine sulfate. *Heart Lung* **1999**, *28*, 418−428.

(30) Kabanov, A. V.; Felgner, P. L.; Seymour, L. W. *Self-Assembling Complexes For Gene Delivery: From Laboratory to Clinical Trial*; John Wiley & Sons: Chichester, U.K., 1998; pp 197−218.

(31) Grosberg, A. Y.; Nguyen, T. T.; Shklovskii, B. I. Colloquium: The physics of charge inversion in chemical and biological systems. *Rev. Mod. Phys.* **2002**, *74*, 329−345.

(32) Zhang, F.; Weggler, S.; Ziller, M. J.; Ianeselli, L.; Heck, B. S.; Hildebrandt, A.; Kohlbacher, O.; Skoda, M. W. A.; Jacobs, R. M. J.; Schreiber, F. Universality of protein reentrant condensation in solution induced by multivalent metal ions. *Proteins* **2010**, *78*, 3450−3457.

(33) Tantra, R.; Schulze, P.; Quincey, P. Effect of nanoparticle concentration on zeta-potential measurement results and reproducibility. *Particuology* **2010**, *8*, 279−285.

(34) Kaszuba, M.; Corbett, J.; Watson, F. M.; Jones, A. High-concentration zeta potential measurements using light-scattering techniques. *Philos. Trans. R. Soc., A* **2010**, *368*, 4439−4451.

(35) Medrzycka, K. B. The effect of particle concentration on zeta potential in extremely dilute solutions. *Colloid Polym. Sci.* **1991**, *269*, 85−90.

DOI: 10.1021/acs.langmuir.8b03927
Langmuir 2019, 35, 4146−4151

(36) Davies, R. T.; Kim, J.; Jang, S. C.; Choi, E.-J.; Gho, Y. S.; Park, J. Microfluidic filtration system to isolate extracellular vesicles from blood. *Lab Chip* **2012**, *12*, 5202−5210.
(37) Christensen, S. M.; Stamou, D. Surface-based lipid vesicle reactor systems: fabrication and applications. *Soft Matter* **2007**, *3*, 828−836.
(38) Alheshibri, M.; Qian, J.; Jehannin, M.; Craig, V. S. J. A history of nanobubbles. *Langmuir* **2016**, *32*, 11086−11100.
(39) Seddon, J. R. T.; Lohse, D.; Ducker, W. A.; Craig, V. S. J. A deliberation on nanobubbles at surfaces and in bulk. *ChemPhysChem* **2012**, *13*, 2179−2187.
(40) Postnikov, A. V.; Uvarov, I. V.; Lokhanin, M. V.; Svetovoy, V. B. Electrically controlled cloud of bulk nanobubbles in water solutions. *PLoS One* **2017**, *12*, No. e0181727.
(41) Epstein, P. S.; Plesset, M. S. On the Stability of Gas Bubbles in Liquid−Gas Solutions. *J. Chem. Phys.* **1950**, *18*, 1505−1509.

DOI: 10.1021/acs.langmuir.8b03927
Langmuir 2019, 35, 4146−4151